Metal homoepitaxial growth at very low temperatures: Lattice-gas models with restricted downward funneling

K. J. Caspersen[1] and J. W. Evans[2]
[1]*Department of Chemistry and Ames Laboratory, Iowa State University, Ames, Iowa 50011*
[2]*Department of Mathematics and Ames Laboratory, Iowa State University, Ames, Iowa 50011*
(Received 23 January 2001; published 10 July 2001)

We develop and analyze $1+1$- and $2+1$-dimensional (d) models for multilayer homoepitaxial growth of metal films at low temperatures (T), where intralayer terrace diffusion is inoperative. This work is motivated by recent variable-temperature scanning tunneling microscopy studies of Ag/Ag(100) homoepitaxy down to 50 K. Adsorption sites are bridge sites in our $1+1d$ models, and fourfold hollow sites in our $2+1d$ models for fcc(100) or bcc(100) surfaces. For growth at 0 K, we introduce a ''restricted downward funneling'' model, wherein deposited atoms can be trapped on the sides of steep nanoprotrusions rather than always funneling down to lower adsorption sites. This leads to the formation of *overhangs* and *internal defects* (or *voids*), and associated ''rough'' growth. Upon increasing T, we propose that a series of interlayer diffusion processes become operative, with activation barriers below that for terrace diffusion. This leads to ''smooth'' growth of the film for higher T (but still within the regime where terrace diffusion is absent), similar to that observed in models incorporating ''complete downward funneling.''

DOI: 10.1103/PhysRevB.64.075401 PACS number(s): 68.55.Jk, 68.35.Fx, 68.35.Ct

I. INTRODUCTION

A traditional expectation for homoepitaxial growth is that the roughness of deposited films of a given thickness should increase with decreasing deposition temperature (T), due to enhanced kinetic barriers to smoothing.[1,2] However, unexpected ''smooth growth'' has been observed in diffraction studies[3,4] of metal (100) homoepitaxial growth at liquid-nitrogen temperatures where terrace diffusion is inoperative. This behavior was initially associated with ''transient mobility'' of ''hot'' deposited adatoms.[3] However, such transient mobility was not observed in molecular-dynamics (MD) studies. An alternative proposal was that the smooth growth was due to ''downward funneling'' (DF) of depositing atoms from the point of impact to lower fourfold hollow sites in the fcc (100) crystal geometry.[5] It should be noted, however, that the DF model does not explain the narrow diffraction profiles (i.e., long-range lateral spatial correlations) observed in the submonolayer regime.[6]

Recent variable-temperature scanning tunneling microscopy (VTSTM) studies[7–9] of the morphology of 25–30 monolayer (ML) Ag films deposited on Ag(100) do in fact find ''re-entrant'' smooth growth. Specifically, the roughness increases as the deposition temperature is lowered from room temperature to 210 K, but then decreases again until about 140 K. The smooth growth observed at 140 K is consistent with the earlier diffraction studies.[3,4] Furthermore, the measured roughness is just slightly above that predicted by the downward funneling model with no thermal diffusion processes[5] (if one corrects the continuous STM height distribution to account for discrete atomic layers[9]). However, the VTSTM studies in Refs. 7 and 9 examine roughness down to 50 K, and reveal a previously unobserved rougher growth for these ''very low'' T. The latter behavior cannot be explained by the downward funneling model without thermal diffusion processes (for which there is no temperature dependence), and suggests that in some growth regimes, this model oversimplifies the atomistic dynamics.

Thus our goal in this paper is the development and analysis of a refined model which can describe the observed novel growth behavior for low T where terrace diffusion is inoperative. Motivated by molecular dynamics studies,[5,10,11] we propose that ''rough growth'' at 0 K can be described by a ''restricted downward funneling'' (RDF) model, where deposited atoms get caught on the sides of steep nanoprotrusions (which are prevalent below 120 K). As a result, overhangs and internal defects or voids can form in the growing film. These RDF models are then extended to describe growth for a range of ''low'' $T>0$ K, where terrace diffusion of isolated adatoms is still inoperative. This is done by incorporating various thermally activated interlayer atomic hopping processes with barriers lower than that for terrace diffusion. Apart from physical $2+1$-dimensional (d) systems of interest, we also present a corresponding $1+1d$ model as it is easy to implement, and the behavior is instructive. The emphasis in this work is not on asymptotic behavior, but rather on experimentally relevant properties of thin films and their variation with T.

In Sec. II, we provide some background on the characterization of film morphology for the relevant (non-simple-cubic) crystalline geometries. Then, in Sec. III, we develop and analyze RDF models for 0 K growth. Next, in Sec. IV, we develop and analyze models for growth in the low-T regime where low-barrier interlayer diffusion processes, but not terrace diffusion, are operative. Some general discussion of observed behavior in the context of coarse-grained continuum modeling is provided in Sec. V, and brief concluding remarks are presented in Sec. VI.

II. CRYSTALLINE GEOMETRY AND MORPHOLOGICAL CHARACTERIZATION OF FILMS

Most lattice-gas modeling of epitaxial growth is based on an unphysical simple cubic (sc) crystalline geometry. For

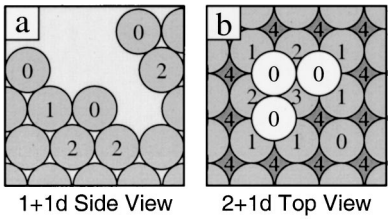

FIG. 1. Schematic of different types of surface atoms (labeled by γ in a subset of cases) for: (a) $1+1d$ (where one example of a bridge site is above the left-most atom labeled $\gamma=2$); (b) $2+1d$ (where fourfold hollow sites are above all atoms labeled by $\gamma=4$).

growth of defect free films with such sc geometries, adsorption sites are chosen as ''on-top'' sites. In other models, such as ballistic deposition,[12] which incorporate defects, atoms can also stick at unsupported sites adjacent to film atoms (which is somewhat artificial), thus creating overhangs. In both cases, atoms in the film are arranged in columns, and the ''surface atoms'' at the top of each column are completely exposed.

The situation is very different for $2+1d$ homoepitaxial growth on fcc (100) or bcc (100) substrates. In the typical situation of defect-free growth, the ''natural'' adsorption sites are fourfold hollow sites supported by four atoms in the layer beneath. Similarly, in the $1+1d$ analogs of these physical geometries, the ''natural'' adsorption sites are bridge sites, supported by two atoms in the layer beneath (see Fig. 1). In our growth models, although deposited atoms will be restricted to epitaxial sites, they will *not* be constrained to sit at natural adsorption sites (i.e., they can have *less* than four supporting atoms in the $2+1d$ models, and *less* than two in $1+1d$ models). In any case, atoms in the film are arranged in vertical columns, and we describe the atoms at the *top* of these columns as ''*surface atoms*.'' Atoms in each column are either in layers of even height, or of odd height (in contrast to sc geometries), and columns of atoms with even and odd height alternate. Also differing from sc geometries is the feature that surface atoms can be partially covered by $\gamma=1-4$ atoms in one of the higher layers in $2+1d$ models (or by $\gamma=1-2$ atoms in $1+1d$ models), or completely exposed ($\gamma=0$). Thus surface atoms are naturally labeled by γ (see Fig. 1). Below, we define the standard quantities used to characterize the *film surface*[12] in terms of the locations of these surface atoms, thereby incorporating refinements necessary to account for non-sc geometries, and for possible internal defects in the growing film.

To characterize *vertical structure* of the film, let $P_{j\gamma}$ denote the fraction of surface atoms which are in layer j and have type γ, so that $\Sigma_j\Sigma_\gamma P_{j\gamma}=1$. It is natural to weight the significance of surface atoms in determining film roughness, etc., according to the degree to which they are covered (i.e., their type γ), as determined by a factor $f_\gamma \leqslant 1$ with $f_0=1$. Then, $P_j=\Sigma_\gamma f_\gamma P_{j\gamma}$ is the effective population of surface atoms in layer j (i.e., the discrete film height distribution), and in general $\Sigma_j P_j$ depends on film structure. Below, we shall utilize the normalized height distribution, $P'_j=P_j/\Sigma_j P_j$. Of course, the choice of f_γ is somewhat arbitrary, but one natural possibility is to set $f_\gamma=(2n-\gamma)/(2n)$ for the $n+1$-dimensional systems with $n=1$ or 2. Then f_γ varies between unity for fully exposed surface atoms ($\gamma=0$), and zero for the maximum α. Furthermore, for films with *no* overhangs or defects, one has the familiar result, $2P_j=\theta_j-\theta_{j+1}$, analogous to behavior for the sc geometry.[13]

The following quantities characterizing the vertical structure of the film surface are primary interest: the mean film height $j_{\rm av}$; the interface width W (both in units of the vertical interlayer spacing); the skewness κ; and the kurtosis Q, of the film height distribution. We define these quantities by

$$j_{\rm av}=\Sigma_j jP'_j \quad W^2=\Sigma_j(j-j_{\rm av})^2P'_j$$

$$\kappa=W^{-3}\Sigma_j(j-j_{\rm av})^3P'_j, \tag{2.1}$$

$$\text{and} \quad Q+3=W^{-4}\Sigma_j(j-j_{\rm av})^4P'_j.$$

Since the P'_j are based on surface atoms, these quantities effectively ignore any enclosed voids. W measures roughness of the film surface, κ gives a measure of vertical asymmetry, and Q measures the weight of the height distribution in the tail, relative to a Gaussian where $Q=0$. We consider deposition to be initiated on a perfect flat substrate, so one has $j_{\rm av}\geqslant Ft=\theta$, where F is the deposition flux in ML/unit time, t is the duration of deposition, and θ is the coverage in monolayers (ML's). The equality applies for *no* internal voids. Also, one generally expects that $W=W(L,t)\sim L^\alpha f(t/L^z)$, for a system of linear size L (with periodic boundary conditions), where $f(x\ll 1)\sim x^\beta$, with $\beta=\alpha/z$, and $f(x\gg 1)\sim$constant.[12] Thus for $L\to\infty$, one has $W\sim t^\beta$ for large t, corresponding to ''kinetic roughening'' of the growing film (for $\beta>0$). In some models, one has slower roughening where $W^2\sim\ln(t)$, for which one usually identifies $\beta=0$. For $t\to\infty$, the saturation roughness in a finite system satisfies $W\sim L^\alpha$. The behavior of κ and Q will be discussed below for specific models.

It is also appropriate to characterize the *lateral structure* of the film surface. To his end, one introduces a height-difference correlation function, $H(r)$. This quantity gives the mean-square height difference for lateral separations r, and is defined by

$$H(r)=\Sigma_{j\,k}(j-k)^2P'_{j\,k}(r). \tag{2.2}$$

Here, $P'_{j\,k}(r)$ is the pair probability for surface atoms in layers j and k to be separated laterally by r, normalized so that $\Sigma_{j\,k}P'_{j\,k}(r)=1$. We incorporate the same weighting of surface atoms as in the height distribution. For a specific r, we emphasize that for nonzero $P'_{j\,k}(r)$, the difference in layer labels, j-k, is either constrained to even values (these r are denoted r_+), or to odd values (these r are denoted r_-). Thus we have $P'_{j\,k}(r_+)=0$ for j-k odd, and $P'_{j\,k}(r_-)=0$, for j-k even. This complicates the standard analysis of asymptotic behavior for large r.[12] Nonetheless, one can show that

$$H(r_\pm)\to 2[W^2\pm M_2M_0\pm(M_1)^2]/[1\pm(M_0)^2],$$

$$\text{as} \quad r=|r_\pm|\to\infty, \tag{2.3}$$

where $M_k=(\Sigma_{j\ \mathrm{even}}-\Sigma_{j\ \mathrm{odd}})j^k P'_j$ ($\sim W^{k-1}$ in some situations);[14] see the Appendix. Thus one has $H(r)\to 2W^2$ except for a ''small'' correction, for large W. This mimics standard behavior for sc geometries where $H(r)\sim r^{2\alpha}$ for $r \ll \xi \sim t^{1/z}$, and $H(r)\approx 2W^2$ for $r \gg \xi$.[12]

III. ''RESTRICTED DOWNWARD FUNNELING'' MODELS FOR GROWTH AT 0 K

For temperatures at or very close to 0 K, *all* thermal diffusion processes are inactive, so the structure of growing films (and specifically their surface morphology), is controlled by the deposition dynamics. As noted in Sec. I, a commonly accepted view is that smooth growth for fcc (100) metal homoepitaxy at low-T derives from the downward funneling (DF) of atoms depositing at step edges and on the sides of nanoprotrusions to lower fourfold hollow adsorption sites in the fcc (100) crystal geometry.[5,15] For DF, deposited atoms require the maximum possible number (four) of support atoms, and if the impact a site that has fewer, they deflect or funnel downward until reaching such a site. Indeed, models for growth at higher T do reveal ''re-entrant'' smooth growth at lower T if DF deposition dynamics is incorporated.[7,9,16,17] However, as also indicated in Sec. I, experimental W values for 25 ML Ag/Ag(100) films deposited at around 50 K (and presumably also for lower T) are significantly higher than DF values. We believe that these high W values can only be described by modifying the DF deposition dynamics. Thus we introduce the concept of ''restricted downward funneling'' (RDF) deposition dynamics: atoms depositing on the sides of nanoprotrusions do not necessarily funnel down to lower fourfold-hollow sites, but rather can adhere to or get stuck at ''trap sites'' on these sides that do not necessarily have four support atoms. Specifically, after impact, one checks to see if the site is in this set of specified trap sites; if not the atom funnels downward to an available adjacent site in the next lower layer, checking again for a trap site, and continuing this process until such a site is reached. These models are motivated by molecular dynamics studies which reveal the trapping of adatoms depositing on {111} facets forming the sides of nanopyramids placed on a fcc (100) surface.[10] One consequence of this breakdown of funneling is the possibility of forming overhangs and internal defects in the growing film, a feature which is incorporated into our modeling, and which has also been observed in molecular dynamics studies of film growth at low T.[11]

While detailed analysis of experiments requires a model with the correct dimensionality $(2+1d)$, we will also discuss analogous $1+1d$ models involving adsorption at bridge sites [see Fig. 1(a)]. The DF model in $1+1d$ has been implemented previously,[5,15,18] and modification to incorporate RDF is natural and straightforward. The lower dimensional models can provide insight into behavior for the physically relevant higher dimension. Before proceeding, it is convenient to introduce a simple notation to characterize trap sites in the various RDF (or DF) models. They will be labeled by ns\nn, where ns number of support atoms, and nn is the *minimum* number of adjacent in-layer atoms (for the specified ns) needed to trap a deposited atom. Thus for the DF model, the only trap sites are 4\0 in $2+1d$, and 2\0 in $1+1d$. Below, we present detailed results from kinetic Monte Carlo simulation of RDF models, and compare behavior with that of DF models.

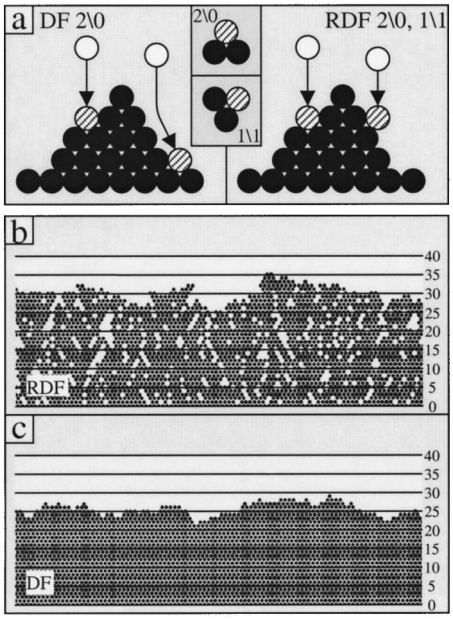

FIG. 2. (a) Schematic of DF and RDF dynamics in $1+1d$. Hatched sites are final trap sites (which are labeled for RDF in the central inset). Simulated 25-ML films in $1+1d$ for (b) RDF; (c) DF.

A. 1+1-DIMENSIONAL MODELS

Trap sites in our RDF model are naturally designated as either 2\0 or 1\1 sites, as compared with only 2\0 sites for DF. See the schematic in Fig. 2(a). Also shown in Figs. 2(b) and (c) are examples of 25-ML films simulated in these models. Simulation results related to the first few moments of the height distribution are shown in Fig. 3. Perhaps of primary interest is behavior of the roughness W. For a large system, RDF and DF models show the same behavior for low θ until significant higher layer population is achieved. Subsequently, distinct behavior emerges, and asymptotic scaling is achieved fairly quickly after $\theta \approx 10$ ML. We find that $\beta=0.31(\approx\frac{1}{3})$ for RDF, and $\beta=0.25(\approx\frac{1}{4})$ for DF. This is consistent with expectations from coarse-grained continuum treatments of these models, which indicate that Kardar-Parisi-Zhang (KPZ) behavior will be observed for RDF, and Edwards-Wilkinson (EW) behavior for DF (see Sec. V). From the saturation roughness versus system size, $L \geqslant 100$ (lattice constants), we find the expected values for roughness exponents of $\alpha=0.50\pm0.02$ for RDF, and $\alpha=0.50\pm0.001$ for DF (see Sec. V). Another basic quality for RDF is the defect density (per site), which we simply define as $\rho_d=(j_{\mathrm{av}}-\theta)/j_{\mathrm{av}}$. Initially, ρ_d increases slowly (since building a void requires several deposited atoms), and then approaches monotonically its asymptotic value of about 0.18.

Next, we discuss the θ dependence of κ and Q. For both

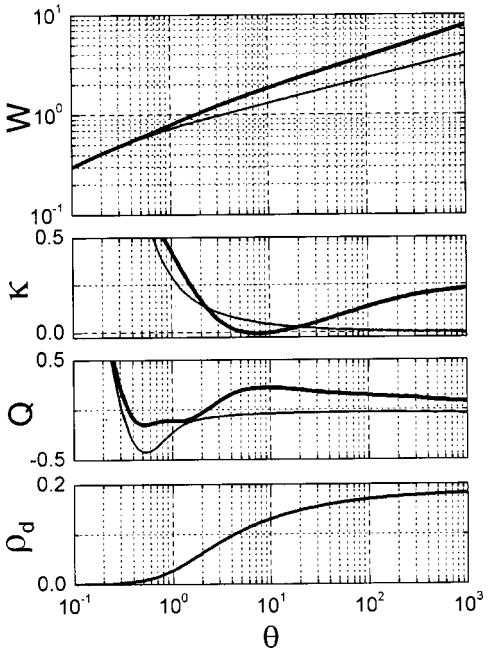

FIG. 3. W, κ, Q, and ρ_d versus θ for the RDF model (thick solid line) and the DF model (thin solid line) for 0 K growth in $1+1d$. All quantities are dimensionless (and $\rho_d=0$ for DF).

models, one has $\kappa \sim \theta^{-1/2}$ and $Q \sim \theta^{-1}$, for $\theta \ll 1$, corresponding to initial population of effectively only the first layer. For DF, κ decreases monotonically to zero (as expected for EW), although rather slowly. The finer details of this behavior may reflect the sensitivity of odd moments of the height distribution (like κ) to our choice of f_γ quantifying surface atom exposure.[19] For RDF, κ decreases until about 10 ML, and then appears to increase towards the asymptotic KPZ value of 0.294.[20] The initial trend likely reflects the feature that RDF initially has difficulty filling lower surface sites leaving large crevasses on the surface (decreasing κ). Eventually, overhangs and protrusions form covering the crevasses, and leading to an increase in κ. For both models, Q shows the same features: an initial decrease in Q to a minimum value (reflecting limitations on building microprotrusions at low θ), and then appears to approach its asymptotic EW value of 0 for DF, and KPZ value of 0.165 for RDF.[20]

Finally, in the top frames of Fig. 4, we show examples of the behavior of $H(r)$ versus r (in units of the surface lattice constant) for the $1+1d$ DF and RDF models. Note the appearance of ''oscillations'' (which are most clear for small W), consistent with Eq. (2.3).

B. 2+1-dimensional models

Our $2+1d$ studies are performed for a crystalline geometry corresponding to an fcc (100) surface. Thus the only trap sites for DF model are the 4\0 (fourfold hollow) sites. In contrast, for RDF, we allow 3\0 trap sites with only three support atoms, 2\1 trap sites with two support atoms, provided they had at least one in-layer nearest neighbor, and even 1\2 trap sites with one support atom and at least two

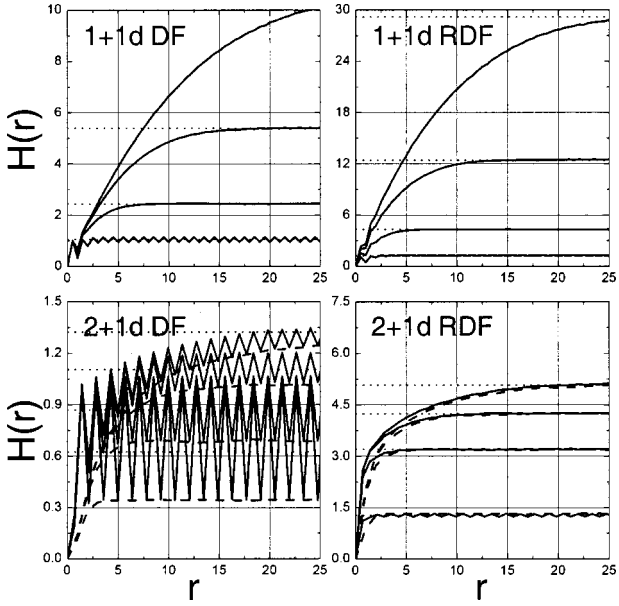

FIG. 4. Top frames: $H(r)$ versus r in the $1+1d$ DF and RDF models. Bottom frames: $H(r)$ versus r in the $2+1d$ DF and RDF models. The solid (dashed) lines correspond to the [110] ([100]) directions. In all cases, behavior for four coverages (1, 5, 25, 100 ML's from bottom to top) are shown. $H(r)$ is dimensionless (based on units of the interlayer spacing), and r is dimensionless (units of surface lattice constant). Horizontal dotted lines give values of $2W^2$.

in-layer nearest neighbors.[21] A schematic of these trap sites for the DF and RDF models is provided in Fig. 5(a), along with a cross section of simulated 25-ML films in Figs. 5(b) and 4(c). Simulation results related to the first few moments of the height distribution are shown in Fig. 6. Behavior is

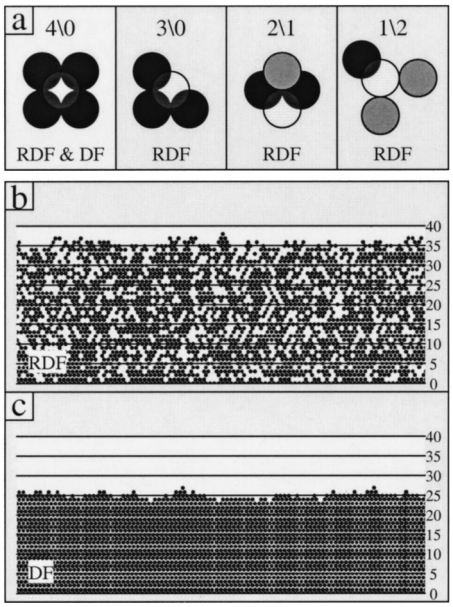

FIG. 5. (a) Schematic of trap sites (open circles) for RDF in $2+1d$. Support atoms are dark circles, and in-layer neighbors are gray. Simulated 25-ML films in $2+1d$ for (b) RDF; (c) DF.

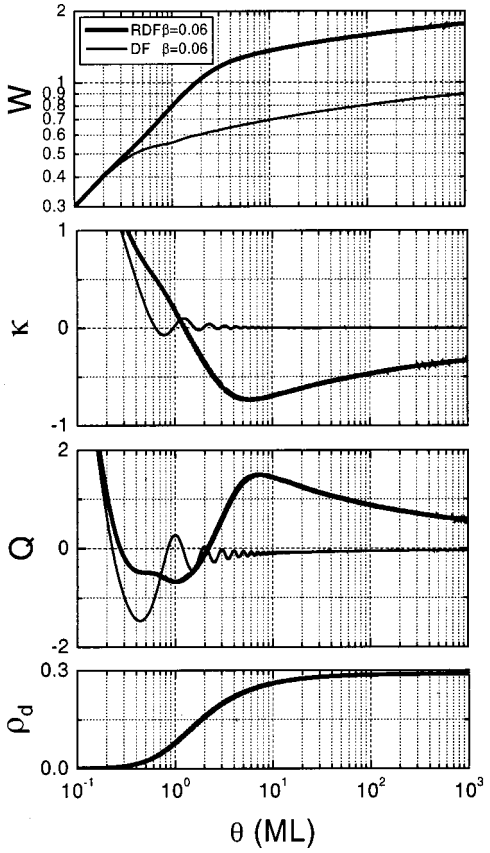

FIG. 6. W, κ, Q, and ρ_d versus θ for the RDF model (thick solid line) and the DF model (thin solid line) for 0 K growth in $2+1d$. All quantities are dimensionless (and $\rho_d=0$ for DF).

qualitatively similar to $1+1d$, but there are some significant quantitative differences. Increased pathways for funneling, and constraints in population of higher layers, creates smoother surfaces for both models. The *effective* β (at around 10^3 ML) is significantly reduced to about 0.06. This is expected for DF in $2+1d$ where EW with $\beta=0$ applies. The RDF model does not exhibit asymptotic KPZ behavior where $\beta\approx 0.24$,[12] an issue to be discussed further in Sec. V. For RDF (DF), effective values for α decrease from 0.13 (0.14) for $L=15-35$ to 0.10 (0.11) for $L=35-70$ for RDF. This should be compared with asymptotic values of $\alpha=0$ for EW, and $\alpha=0.4$ for KPZ, although lower values down to 0.2 often emerge from simulations for the latter.[12] For RDF, the defect density, again defined as $\rho_d=(j_{\rm av}-\theta)/j_{\rm av}$, increases monotonically (slowly initially) as in $1+1d$, achieving an asymptotic value of about 0.29 (although more quickly than in $1+1d$).

For DF, oscillations appear in κ and Q reflecting sensitivity of these quantities to the initial quasi-layer-by-layer growth, and then these quantities decay quickly to around zero (as expected for EW). For RDF, the development of a ''large'' negative κ and positive Q achieved at $\theta\approx 8$ ML reflect the development of deep crevasses, and the limited inability of growth to cover these by developing microprotrusions and overhangs. For larger θ, both quantities decrease in amplitude which might be compared with asymptotic EW values of zero.[22]

Finally, in the bottom two frames of Fig. 4, we show examples of the behavior of $H(r)$ versus r for the $2+1d$ DF and RDF models. Solid lines correspond to the direction of [100] steps along diagonal rows of surface atoms, where atoms in adjacent columns alternate between even on odd layers. These reveal the appearance of ''oscillations'' (for small W), consistent with Eq. (2.3). Dashed lines correspond to r in the direction of [110] steps, where atoms in the relevant columns are either all in even or all in odd layers, so there are no oscillations in $H(r)$.

IV. GROWTH AT LOW TEMPERATURES: LOW-BARRIER INTERLAYER DIFFUSION

In this section, we will discuss deposition at temperatures above 0 K, but still below the threshold for activation of the terrace diffusion of isolated adatoms. Why should there be any temperature dependence to growth? We argue that typically there should exist a family of low-barrier interlayer thermal diffusion processes which are active, and which combined with the deposition dynamics control film growth in this low-T regime. These low-barrier processes consist of diffusion from the low coordination sites that are created as a result of the RDF deposition dynamics. Our motivation for this model comes from consideration of the Ag/Ag(100) system, where the barrier for diffusion across {100} terraces equals $E_d^{(100)}\approx 0.4$ eV,[23] so this process is inactive below about 130 K. However, the barrier for diffusion across {111} micofacets of $E_d^{(111)}\approx 0.1$ eV (Ref. 24) is much lower, leading to activation of this process around 40 K. Atoms landing on the side of pyramidal microprotrusions are, in actuality, landing on {111} facets, so their diffusion leads to interlayer transport potentially smoothing the film above 40 K. In the rest of this section, we present results of the kinetic Monte Carlo (KMC) simulations, in which we incorporate certain low-barrier diffusion processes into our previously described RDF models in $1+1d$ and $2+1d$. Using parameters for Ag/Ag(100) in the $2+1d$ model, we shall see that activation of these interlayer diffusion processes leads to smoother film growth as T is increased from 0 K to around 100 K, consistent with experimental observations.[7,9]

A. 1+1-dimensional models

In our model, atoms are randomly deposited via RDF dynamics at a rate F ML/unit time, and then certain lower-coordination atoms undergo interlayer hopping to adjacent sites until reaching designated trapping sites (such as 2\0 bridge sites). A detailed specification of hopping is naturally given in terms of the (initial) coordination, $m_i=1-6$, of deposited atoms in this $1+1d$ geometry. Atoms with $m_i=1$ are specified to hop instantaneously, consistent with low barrier expected for these sites. Atoms with $m_i=2$ (except those at 2\0 sites with both support atoms) are given a finite hop rate h unit time (per direction). All other atoms ($m_i>2$ or 2\0) are not allowed to diffuse, consistent with the high barriers expected for high coordination, and emulating the feature of the $2+1d$ system that terrace diffusion is inactive in the temperature range of interest. Atoms were only allowed

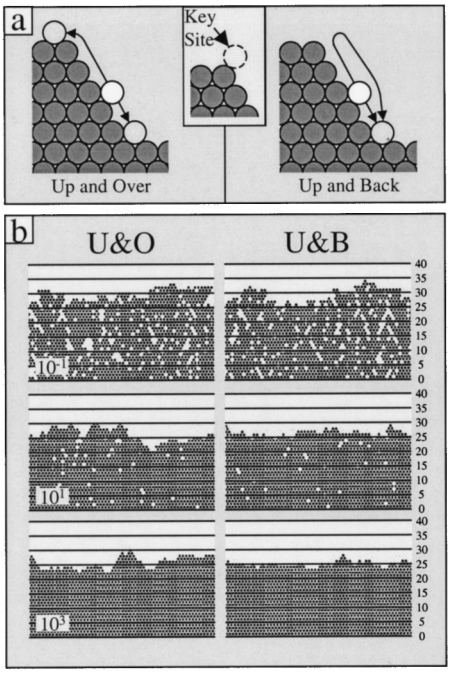

FIG. 7. (a) Schematic of U&O and U&B models in $1+1d$. The inset shows the key ''transition state'' accessible only in the U&O model. (b) Simulated 25-ML films for $h/F=10^{-1}$, 10^{0}, 10^{3} (shown).

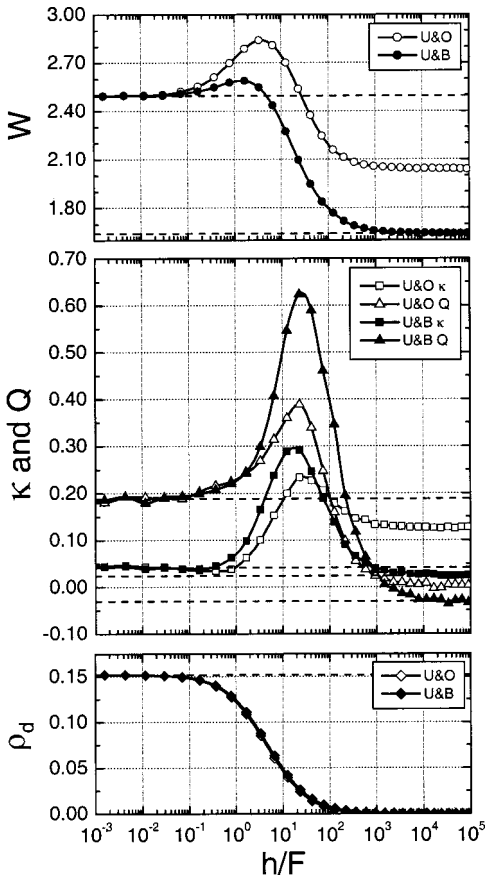

FIG. 8. W, κ, Q, and ρ_d versus h/F for 25-ML films for the U&O model (small open symbols) and the U&B model (small closed symbols) in $1+1d$. All quantities are dimensionless. The horizontal dashed lines indicate either 0 K RDF values or DF values for various quantities.

to hop to one of the six unoccupied nearest-neighbor (final) destination sites, in which the coordination satisfied $m_f>0$. This last requirement ensures that diffusing atoms do not leave the surface.

We designate the above prescription as the ''up and over'' (U&O) model, since atoms can climb from the sides to the top of mesas through a $m_f=1$ ''transition state'' site [as shown in Fig. 7(a)]. The corresponding process in physical $2+1d$ systems is expected to have a substantial barrier (see Sec. IV B), so we are motivated to also consider a modified ''up and back'' (U&B) model where this process is inoperative [see Fig. 7(a)]. This modification is achieved by simply imposing the restriction that $m_f>1$, blocking atoms from hopping into the above-mentioned transition state.

As there is only a single finite hopping rate h in our models, film structure (for a given θ) is determined entirely by the ratio h/F. Figures 7(b) and 8 show the variation with h/F of key features of 25-ML films generated from KMC simulations in the $1+1d$ U&O and U&B models. Below we describe the observed behavior for various regimes of h/F:
(i) *Negligible diffusion*. For h/F below 10^{-1}, deviations from 0 K RDF growth are negligible.
(ii) *Onset of diffusion*. For h/F around $10^{-1}-10^{0}$, diffusion becomes active on the time scale of deposition, but each diffusing atom hops approximately only once before it is stabilized. We now discuss the observed deviations or perturbations of the 0 K RDF morphology. Diffusion of atoms to trap sites in higher or lower layers has the effect of increasing not just the width (W) of the height distribution, but also the relative population in the upper and lower extremes or tails (i.e., increasing Q). The significant increase in W is not surprising for the U&O model (allowing for climbing on top of mesas), but a small increase occurs even for U&B dynamics. The change in skewness κ is less dramatic. An initial slight decrease in κ for U&B dynamics may reflect an initial bias towards lower trap sites, whereas the initial increase in κ for U&O dynamics reflects the possibility of populating higher trap sites by climbing on top of mesas.
(iii) *Significant diffusion*. The range $10^{0}-10^{1}<h/F<10^{3}-10^{4}$ is characterized by a complex interplay between RDF (creating voids and overhangs), and the increased diffusivity (filling in voids). Increased diffusivity allows atoms to more easily find higher coordinated trap sites, eliminating voids and overhangs, and decreasing in W. More surprising is the nonmonotonic behavior of κ and Q. Apparently for $h/F<20$, the combined effect of RDF and diffusion is to produce a few broad protrusions while reducing W. These contribute to the upper extreme of the height distribution, thus increasing κ as well as Q. For $h/F>20$, diffusion is sufficiently fast to preclude RDF from building many of these protrusions, thus decreasing κ and Q.
(iv) *Rapid diffusion (asymptotic regime)*. For $h/F>10^{3}-10^{4}$, diffusion is so rapid that deposited atoms can effectively always find a trap site without interference from subsequent deposited atoms. In this regime, U&O dynamics reduces to model in which atoms are immediately placed at

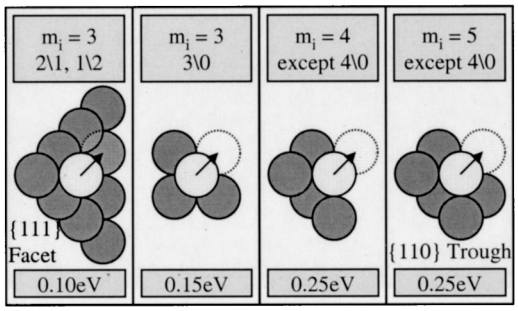

FIG. 9. Schematic of low-barrier interlayer hops in $2+1d$, together with the associated barriers.

one of the trap-sites on either side of the deposition site, whether it be above or below. In contrast, the restriction that $m_f>1$ for the U&B model means that atoms go to the lower trap site, so it reduces to the DF model in this regime [see Figs. 7(b) and 8]. In both cases, the films have no overhangs or voids.

B. 2+1-dimensional models

One complication in incorporating interlayer diffusion processes into the 0 K $2+1d$ RDF model is the vast number and variety of configurations with low coordination from which interlayer hopping (with low barrier) may be possible. Furthermore, it is likely that a spectrum of activation barriers E_d, and thus Arrhenius rates, will apply for diffusive hopping. Thus we make some reasonable, simple choices for these barriers based partly on the coordination of the atom, as well as on known results for the Ag system. Adatoms in sites with a very low (initial) coordination of $m_i=1$ or 2 likely have an extremely low barrier towards diffusion, and thus are prescribed to hop instantaneously. Some adatoms with $m_i=3$ are on the {111} microfaceted sides of pyramidal microprotrusions on the {100} surface, and thus have $E_d=0.10\,\mathrm{eV}$ corresponding to terrace diffusion of Ag on Ag(111).[24] In fact, we assign $E_d=0.10\,\mathrm{eV}$ to all sites with $m_s=3$, except for 3\0 sites. The latter more resemble 4\0 sites, which have a high barrier, and are therefore assigned $E_d=0.15\,\mathrm{eV}$. Hopping of adatoms from some sites with $m_s=4$ resembles dimer scission on a Ag(111) surface where $E_d\approx 0.25\,\mathrm{eV}$,[25] so sites with $m_i=4$ (except 4\0 sites) were assigned this barrier. Hopping of adatoms from some sites with $m_i=5$ resembles in-channel diffusion of Ag on Ag(110) for which $E_d\approx 0.25\,\mathrm{eV}$,[26] so sites with $m_i=5$ (except fourfold hollow sites) were assigned this barrier. Adatoms at sites with $m_i\geqslant 6$ are not allowed to hop, due to assumed high barriers. A schematic of these diffusion processes is shown in Fig. 9. The attempt frequency (ν) for all active hopping processes was set to $1\times 10^{12}\,\mathrm{s}$, consistent estimates for diffusion of Ag on Ag(111).[24] We also set $F=0.04\,\mathrm{ML/s}$ as in experiment,[7] but note that results depend only on the ratio ν/F.

Analogous to $1+1d$, in our $2+1d$ up and over (U&O) model, adatoms are allowed to diffuse to any of the 12 unoccupied nearest-neighbor sites, provided that the (final) coordination satisfies $m_f\geqslant 1$. In particular, this means that they can climb up from the {111} microfaceted sides to the top of pyramidal mesas through the low-coordination ''transition state'' site. However, this corresponds to hopping down from the edge of an island on a Ag(111) surface, for which we know there exists a substantial additional Ehrlich-Schwoebel barrier.[24] Thus it is reasonable to examine the effect of precluding this process in a $2+1d$ up and back (U&B) model, where adatoms can only hop to sites with $m_d\geqslant 3$, thus preventing them from hopping into the above-mentioned transition state.

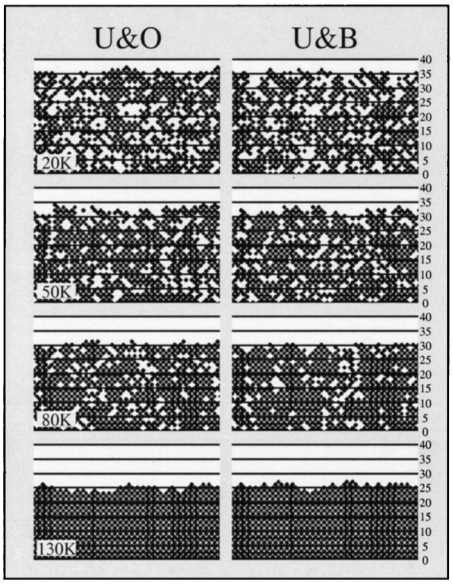

FIG. 10. Simulated 25-ML films for 20, 50, 80, 130 K (shown) for the U&O and U&B models in $2+1d$.

Since there are several rates in the $2+1d$ models, it is natural to examine behavior as a function of deposition temperature T (rather than versus some h/F), thus facilitating comparison with experiment. Figures 10 and 11 show the variation with T of key features of 25-ML films generated from KMC simulations in the $2+1d$ U&B and U&O models. The most dramatic feature of Fig. 11 is the step-wise variation of quantities with increasing T; the three steps correspond to the activation of three different classes of diffusion processes with progressively higher barriers (0.10, 0.15, and 0.25 eV). First, we discuss the variation of W with T. For the U&O model, the steps at 40 K (activation of diffusion on {111} facets) and at 105 K (activation of diffusion for $m_i=4$ or 5) display a transient increase in W, since the activated process allows adatoms to climb on top of mesas and become trapped on top. In contrast, the step at 60 K (activation of diffusion from 3\0 sites) shows no such increase. This is because upward hopping from 3\0 sites is not possible (destination sites would have $m_f=0$, i.e., no support). Similarly, W decreases monotonically with increasing T for the U&B model, where climbing on top of mesas is precluded. For high T (>120 K), effectively all deposited atoms find a trap site without interference from subsequent deposition. Not surprisingly, $W(T>120\,\mathrm{K})$ for the U&O model is ''quite high,'' as a significant fraction of these trap sites are higher than the deposition site. $W(T>120\,\mathrm{K})$ for the U&B

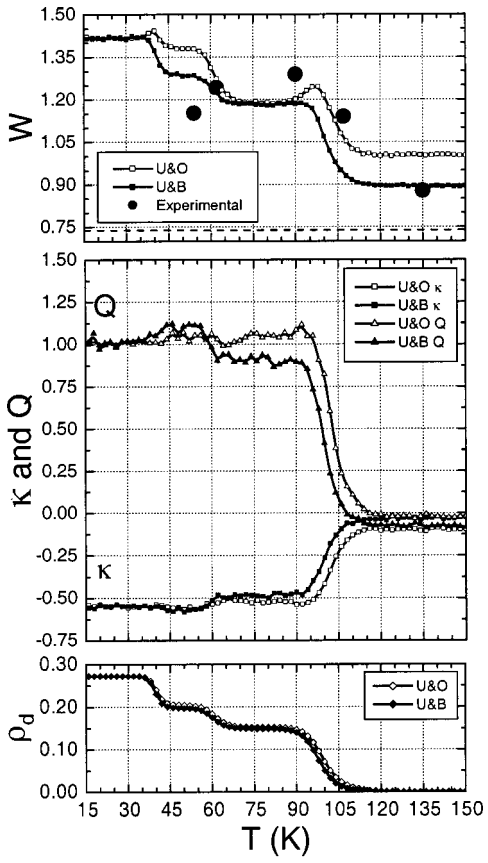

FIG. 11. W, κ, Q, and ρ_d versus T for 25-ML films for the U&O model (open small symbols) and the U&B model (closed small symbols) in $2+1d$. Experimental data for Ag/Ag(100) is also shown (large closed circles). All quantities are dimensionless. The dashed horizontal line in the top frame indicates the DF value for W.

model is lower, but not as low as for the DF model, contrasting $1+1d$ behavior. This is because the higher dimensionality allows for limited lateral diffusion to trap sites (along the sides of microprotrusions), rather than just downward transport to 4\0 traps as in DF. In both models, as expected, diffusion processes work to eliminate voids and overhangs, the associated density, $\rho_d=(j_{\rm av}-\theta)/j_{\rm av}$, decreasing step-wise monotonically to be effectively zero for $T>120$ K.

To summarize the overall behavior, one sees that both models deviate smoothly from 0 K RDF behavior with increasing T: W decreases towards (but does not achieve) the DF value, κ and Q approach DF-like values, and ρ_d vanishes consistent with the DF. Therefore, the combination of RDF with these very active selected low barrier diffusion process work to produce DF or EW-like behavior for $T>120$ K. Since the actual barrier to climb up on top of mesas is finite, perhaps 0.2–0.3 eV for Ag/Ag(100), the optimum prediction behavior for this system may lie between the U&O and U&B models. In any case, considering the simplicity of these models, predicted behavior of W versus T is in good semiquantitative agreement with experimental results[7,9] for the same deposition flux (see Fig. 11).

V. DISCUSSION: CONTINUUM FORMULATIONS OF FILM GROWTH

To provide some basis for understanding the behavior observed in our RDF models, it is instructive to consider a coarse-grained description of film morphology and growth.[12] Here, one does not resolve atomically discrete lateral *or* vertical film structure, and thus describes film height and lateral position x by a continuous function $h(x,t)$ (defined here with the units of interlayer spacing or monolayers). Then, $h(x,t)$ satisfies stochastic continuum evolution equation of the form

$$\partial/\partial t\, h(x,t)=F/\rho-\nabla\cdot J+\eta, \tag{5.1}$$

where F is the deposition flux in ML/unit time, $\rho=1-\rho_d$ is the film density (normalized to unity for defect free epitaxial growth), and J is the conservative lateral mass current across the film surface. Finally, η denotes the shot noise in the deposition process, and satisfies $\langle\eta\rangle=0$, and $\langle\eta(x,t)\,\eta(x',t')\rangle\propto\delta(x-x')\,\delta(t-t')$, where $\langle\,\rangle$ denotes a suitable ensemble average. For our purposes, the lateral mass flux J is naturally decomposed as $J=J_{\rm DYN}+J_{\rm THERM}$, where the component $J_{\rm DYN}$ is associated with transient deposition dynamics, and the component, $J_{\rm THERM}$, with thermally activated diffusion (for $T>0$ K). Often, one develops expansions in slope (and curvature) for J and ρ, and thus for the right-hand side of Eq. (5.1), focusing on the lowest-order terms which control the long-time and long wavelength asymptotic behavior.[12]

It is convenient to first consider the standard downward funneling (DF) model for growth at 0 K, where $\rho=1$. For surfaces which are fairly smooth locally (small local slopes), it is not surprising that $J_{\rm DYN}=J_{\rm DF}$ should be proportional to the step density, which in turn is proportional to ∇h, so that $J_{\rm DF}\approx -F\nu_{\rm DF}\nabla h$.[15] In fact, simple calculations give quite reliable estimates of $\nu_{\rm DF}$.[17] Then, Eq. (5.1) becomes the linear Edwards-Wilkinson (EW) equation

$$\partial/\partial t\, h(x,t)\approx F-F\nu_{\rm DF}\nabla^2 h+\eta, \tag{5.2}$$

for which $\beta=\frac{1}{4}$ in $1+1d$, and $\beta=0$ (logarithmic roughening) in $2+1d$.[12]

Next, we consider behavior for the restricted downward funneling (RDF) model for growth at 0 K. For small local slopes (where surfaces have primarily monoatomic steps), one expects that to a good approximation, $J_{\rm DYN}=J_{\rm RDF}$ is still proportional to ∇h, so that $J_{\rm RDF}\approx -F\nu_{\rm RDF}\nabla h$. The key difference from the DF model is that now $\rho<1$ due to the formation of internal defects, and one expects that ρ can be expanded as

$$\rho=\rho(\nabla h,\nabla^2 h,\ldots)=\rho_0+\rho_1|\nabla h|^2+\rho_2\nabla^2 h+\ldots. \tag{5.3}$$

Thus Eq. (5.1) becomes the nonlinear Kardar-Parisi-Zhang (KPZ) equation

$$\partial/\partial t\, h(x,t)\approx F(\rho_0)^{-1}-F\rho_1(\rho_0)^{-2}|\nabla h|^2 -F[\nu_{\rm RDF}+\rho_2(\rho_0)^{-2}]\nabla^2 h+\eta, \tag{5.4}$$

for which $\beta=\frac{1}{3}$ in $1+1d$, and $\beta\approx\frac{1}{4}$ for sufficiently strong nonlinearity in $2+1d$.

Some insight into the strength of the nonlinearity comes from studies of the RDF model for deposition on vicinal substrates with a range of prescribed global slopes ∇h_0. Specifically, we monitor the variation in the steady-state defect density with ∇h_0, and find a nearly quadratic variation of the form $\rho(\nabla h_0)\approx\rho_0+\rho_1|\nabla h_0|^2$. From simulations, we determine that $\rho\approx 0.183+0.29|\nabla h_0|^2$ in $1+1d$, and $\rho\approx 0.284+0.065|\nabla h_0|^2$ in $2+1d$. Thus one finds a remarkably weak nonlinearity in $2+1d$ (certainly compared with $1+1d$). This likely explains the slow roughening with $\beta\approx 0.06$ in $2+1d$ over the observed coverage range. One possibility is that asymptotic behavior is not relevant in the experimentally accessed regime, consistent with other models incorporating defects which reveal a very slow crossover to true asymptotic behavior.[27] Another perspective comes from numerical studies of KPZ models in $2+1d$ revealing an apparent kinetic phase transition to a regime of smooth EW growth for sufficiently weak nonlinearity.[12,28] Later work suggested that $2+1d$ was the lower critical dimension for this phase transition,[29] implying that the numerical studies were in fact seeing extremely slow crossover to KPZ behavior. This situation could apply for the RDF model.

We note that there are other standard (on- or off-lattice) ''ballistic deposition'' models which incorporate internal defects or voids, and which do reveal KPZ behavior,[12] similar to our RDF model in $1+1d$. It is also know that introducing some restructuring in these models can significantly modify (and produce ambiguous) asymptotic scaling behavior.[27,30] Yet another example of subtle and complex crossover behavior associated with limited relaxation of depositing particles (even in the absence of voids) is provided by the so-called Wolf-Villain model.[31]

In many models for growth at $T>0$ K which incorporate *thermally activated terrace diffusion*, the associated mass flux is traditionally written in Mullins form as $J_{\rm THERM}=\nabla\mu$, where $\mu=F[\mu_0+\nu'\nabla^2 h+\cdots]$ denotes a generalized chemical potential.[12] Some variations are possible. For example, Stroscio *et al.*[32] suggested replacing $\nabla^2 h$ with $\nabla^4 h$ for systems where terrace diffusion leads to irreversible capture at step edges. Furthermore, the presence of step-edge barriers leads to destabilizing uphill currents, which produce additional slope-dependent contributions to $J_{\rm THERM}$.[12] In all these cases, terrace diffusion is operative leading to the possibility of large lateral characteristic lengths for any film thickness. However, the ''limited'' interlayer thermal diffusion in our models is fundamentally different, being restricted to sloping portions of the film surface, and thus being unable to generate these large lateral characteristic lengths. Thus the form of $J_{\rm THERM}$ is expected to be different from above. For example, in U&B models for high T, RDF plus thermal diffusion together mimic DF, so one has $J_{\rm THERM}=-F\nu_{\rm TH}\nabla h$ (a stabilizing downhill current), where $\nu_{\rm RDF}+\nu_{\rm TH}\approx\nu_{\rm DF}$.

VI. CONCLUSIONS

We have developed $2+1d$ models (and their $1+1d$ analogs) for metal (100) homoepitaxial growth at 0 K controlled by ''restricted downward funneling'' deposition dynamics. These models were extended to describe low-T growth, where terrace diffusion is inoperative, but where various low-barrier interlayer diffusion processes may be active. The $2+1d$ models are quite successful in describing the variation with T (below 130 K) of the roughness of 25-ML Ag/Ag(100) films as observed in recent experiments.[7,9] In particular, they predict the transition from ''smooth growth'' around 115–130 K (effectively described by the simple downward funneling model), to rougher growth at lower T. Furthermore, they predict the incorporation of internal voids or defects in growing metal (100) homoepitaxial films at low T. Indeed, recent experimental evidence for a low density of such defects in Ag/Ag(100) film growth at 100 K was provided by surface-sensitive x-ray scattering studies.[33]

Our models are certainly idealized both in the treatment of the deposition dynamics and of thermally activated diffusion processes. One possible variation in the deposition dynamics is to include ''knock-down'' effects, where for example depositing atoms could knock downhill adatoms caught on the sides of {111} microfacets. Another variation is to implement less restricted funneling, so atoms deposited on sites without four supporting atoms can make at least one downward hop before becoming trapped. These modifications would no doubt reduce the density of internal voids. More generally, behavior would be closer to standard downward funneling model. Possible variations in the treatment of thermal diffusion include incorporation of more precise and more varied barriers for interlayer diffusion processes, and also consistent incorporation of low-barrier interlayer step-edge diffusion processes.[34] The latter will perhaps not much affect W (the main focus of this study), but step-edge diffusion processes should increase the lateral correlation length,[16] and possibly reduce the density of internal voids. This would likely describe more precisely actual experimental behavior.

ACKNOWLEDGMENTS

This work was supported by NSF Grant CHE-0078596, and performed at Ames Laboratory which is operated for the U.S. DOE by Iowa State University under Contract No. W-7405-Eng-82. We thank Paul Miceli, Joachim Krug, and A. Laszlo Barabasi for useful discussions, as well as our experimental collaborators, Conrad Stoldt and Patricia Thiel.

APPENDIX: HEIGHT-DIFFERENCE CORRELATION FUNCTIONS

Let $P'_{j\,k}(r)$ denote the normalized pair probability for surface atoms in layers j and k to separated laterally by $r=r_+$ or r_-, defined as in the text. The independence of film height for two points with an asymptotically large separation implies that $P'_{jk}(r_+)\to c_+P'_jP'_k$ (or 0), for j-k even (or odd), as $|r_+|\to\infty$. Also, one has that $P'_{jk}(r_-)\to c_-P'_jP'_k$ (or 0), for j-k odd (or even), as $|r_-|\to\infty$. Given the normalization condition on $P'_{j\,k}(r)$, it should be clear that the constants of proportionality in these relations are nontrivial, and satisfy

$$(c_+)^{-1}=\Sigma_{j-k\ \mathrm{even}}P'_jP'_k \quad \text{and} \quad (c_-)^{-1}=\Sigma_{j-k\ \mathrm{odd}}P'_jP'_k. \tag{A1}$$

Setting $M_k=(\Sigma_{j\ \mathrm{even}}-\Sigma_{j\ \mathrm{odd}})j^kP'_j$, one can show that

$$(c_+)^{-1}=\tfrac{1}{2}+\tfrac{1}{2}(M_0)^2 \quad \text{and} \quad (c_-)^{-1}=\tfrac{1}{2}-\tfrac{1}{2}(M_0)^2. \tag{A2}$$

Next, we introduce a height-difference correlation function $H(r)$ for lateral separations r defined by

$$H(r)=\Sigma_{jk}(j-k)^2P'_{jk}(r). \tag{A3}$$

The above-mentioned constraint on nonzero $P'_{jk}(r)$ complicates the analysis of $H(r)$. Nonetheless, for asymptotically large r, one can show that

$$H(r_e)\to(c_+)^{-1}\Sigma_{j-k\ \mathrm{even}}(j-k)^2P'_jP'_k = 2[W^2+M_2M_0+(M_1)^2]/[1+(M_0)^2], \tag{A4a}$$

and

$$H(r_0)\to(c_-)^{-1}\Sigma_{j-k\ \mathrm{odd}}(j-k)^2P'_jP'_k = 2[W^2-M_2M_0-(M_1)^2]/[1-(M_0)^2]. \tag{A4b}$$

Finally, we mention another formulation (not used here) for $H(r)$ in non-sc geometries which recovers some of the simpler behavior familiar in sc geometries. The idea is simply to redefine r in a convenient way. For $r=r_+$ separating columns with atoms in both even or both odd layers, the standard definition is used as above. For $r=r_-$ separating atoms in even and odd layers, $r_-=0$ is reassigned to correspond to adjacent columns in a certain direction. Then for each specific $r=r_+$ or r_- take the same set of discrete values, and there is no constraint on $j-k$ being even or odd as above. Thus the analysis of $H(r)$ mimics that for an sc geometry, but now $H(0)>0$.[16]

[1] *Morphological Organization in Epitaxial Growth and Removal*, edited by Z. Zhang and M. G. Lagally (World Scientific, Singapore, 1998).

[2] Another misconception (see Ref. 1) is that smoother growth at low T is simply due to the presence of smaller islands from which deposited atoms can more easily descend.

[3] W. F. Egelhoff and I. Jacob, Phys. Rev. Lett. **62**, 921 (1989).

[4] D. K. Flynn-Sanders, J. W. Evans, and P. A. Thiel, Surf. Sci. **289**, 77 (1993); J. Vac. Sci. Technol. A **7**, 2162 (1989).

[5] J. W. Evans, D. E. Sanders, P. A. Thiel, and A. E. DePristo, Phys. Rev. B **41**, 479 (1990).

[6] Long-range correlations have been attributed to intralayer ''clumping'' of atoms deposited nearby other adatoms, facilitated by low-barrier edge diffusion processes. See M. C. Bartelt and J. W. Evans, Surf. Sci. **423**, 189 (1999); G. Vandoni, C. Felix, R. Monot, J. Buttet, and W. Harbich, *ibid.* **320**, L63 (1994); M. Breeman (unpublished).

[7] C. R. Stoldt, K. J. Caspersen, M. C. Bartelt, C. J. Jenks, J. W. Evans, and P. A. Thiel, Phys. Rev. Lett. **85**, 800 (2000).

[8] G. Constantini, F. Buatier de Mongeot, C. Boragno, and U. Valbusa, Surf. Sci. **459**, L487 (2000).

[9] K. J. Caspersen, C. R. Stoldt, A. R. Layson, M. C. Bartelt, P. A. Thiel, and J. W. Evans, Phys. Rev. B **63**, 085401 (2001).

[10] D. E. Sanders and J. W. Evans, in *Structure of Surfaces III*, edited by S. Y. Tong, M. A. Van Hove, K. Takayanagi, and X. D. Xie (Springer, Berlin, 1991); D. M. Halstead and A. E. DePristo, Surf. Sci. **286**, 275 (1993).

[11] C. Kelchner and A. E. DePristo, Surf. Sci. **393**, 72 (1997).

[12] A. L. Barabasi and H. E. Stanley, *Fractal Concepts in Surface Growth* (Cambridge University Press, Cambridge, 1995).

[13] See the Appendix in J. W. Evans, Phys. Rev. B **39**, 5655 (1989) which normalized P_j to the number of atoms in a complete layer. Here, we normalize to the number of columns (twice as large), hence the extra factor of 2 relating P's and θ's.

[14] If $P'_j\sim W^{-1}f(j/W)$, and $h=W^{-1}$, then $\Sigma_{j\ \mathrm{odd}}j^k\ P'_j\sim W^k\ [h\Sigma_{x=jh(j\ \mathrm{odd})}x^k\ f(x)]$, and similarly with j even. If expressions in parentheses approximate an integral with error $O(h)$, then $M_k\sim W^{k-1}$.

[15] H. C. Kang and J. W. Evans, Surf. Sci. **271**, 321 (1992).

[16] M. C. Bartelt and J. W. Evans, Phys. Rev. Lett. **75**, 4250 (1995).

[17] M. C. Bartelt and J. W. Evans, Surf. Sci. **423**, 189 (1999).

[18] P. Meakin, *Fractals, Scaling and Growth Far From Equilibrium* (Cambridge University Press, Cambridge, 1998). See Fig. 5.8b for an alternative realization of DF in $1+1d$.

[19] Our nonsymmetric choice of $f_\gamma=(2n-\gamma)/(2n)$ for $n+1$ dimensions, atoms at the top ($\gamma=0$) and at the bottom ($\gamma=2n$) of saw-tooth profiles are not weighted equally. A symmetric choice with $f_0=f_{2n}$ would produce modified behavior, perhaps more like in sc geometries.

[20] J. Krug, Adv. Phys. **46**, 139 (1997); M. Prahofer and H. Spohn, Phys. Rev. Lett. **84**, 4882 (2000).

[21] We have checked that behavior of a modified RDF model with only 4\0, 3\0, and 2\1 trap sites is similar to that of the RDF model analyzed here.

[22] For the $2+1d$ ballistic deposition (single-step) model (Ref. 12), κ reaches about 0.7 (-1.3), and Q reaches about 0.3 (0.3) at 10^3 ML's. These models have KPZ scaling.

[23] P. A. Thiel and J. W. Evans, J. Phys. Chem. B **104**, 1663 (2000).

[24] K. Bromann, H. Brune, H. Roder, and K. Kern, Phys. Rev. Lett. **75**, 677 (1995).

[25] J. W. Evans and M. C. Bartelt, in Ref. 1 estimate 0.13 eV for the Ag_2/Ag(111) pair bond energy. For refined estimates, see K. A. Fichthorn and M. Scheffler, Phys. Rev. Lett. **84**, 5371 (2000).

[26] C. Motel, R. Ferrando, F. Hontinfinde, and A. C. Levi, Surf. Sci. **402–404**, 286 (1998).

[27] M. Schimschak and J. Krug, Phys. Rev. B **52**, 8550 (1995); S. Das Sarma, C. J. Lanczycki, S. V. Ghaisas, and J. M. Kim, *ibid.* **49**, 10 693 (1994).

[28] Y. P. Pelligrini and R. Jullien, Phys. Rev. Lett. **64**, 1745 (1990); H. Yan, D. Kessler, and L. M. Sander, *ibid.* **64**, 26 (1990); J. G. Amar and F. Family, *ibid.* **64**, 543 (1990).

[29] T. Natterman and L.-H. Tang, Phys. Rev. A **45**, 7156 (1992).
[30] P. Meakin and R. Jullien, J. Phys. (France) **48**, 1651 (1987).
[31] P. Smilauer and M. Kotrla, Phys. Rev. B **49**, 5769 (1994).
[32] J. A. Stroscio, D. T. Pierce, M. Stiles, A. Zangwill, and L. M. Sander, Phys. Rev. Lett. **75**, 4246 (1995).
[33] W. C. Elliott, P. F. Miceli, and P. W. Stevens, Bull. Am. Phys. Soc. **44**, 1604 (1999).
[34] B. D. Yu and M. Scheffler, Phys. Rev. Lett. **77**, 1095 (1996).